Measurement of a short-wavelength instability in Taylor vortex flow

Michael Dennin, David S. Cannell, and Guenter Ahlers
Department of Physics and Center for Nonlinear Science, University of California, Santa Barbara, Santa Barbara, California 93106
(Received 4 June 1993)

We report experimental results for the stability boundary in Taylor vortex flow for a system with radius ratio 0.5. For most values of the pattern's wave number, quasistatic measurements of the stability boundary are in excellent agreement with the calculation of Paap and Riecke [Phys. Rev. A **41**, 1943 (1990)]. In addition, for large values of the pattern's wave number, performing quenches of the control parameter provided evidence for a new instability which supersedes the usual Eckhaus instability. This new instability is not evident in the quasistatic measurements because of the existence of a nonuniform wave number. We have also observed evidence for this instability with radius ratio 0.74.

PACS number(s): 47.20.Ft, 47.54.+r

I. INTRODUCTION

One of the classical systems for the study of instabilities and pattern formation is Taylor-Couette flow, the flow of a fluid confined between two concentric cylinders. When rotating the inner cylinder about its axis, the initial instability is a transition from a uniform state to a state which is periodic in the axial direction [1]. It is well known that one-dimensional patterns such as this are subject to the long-wavelength Eckhaus instability [2–6]. One of the successes in the study of pattern-forming systems is the agreement between the calculated and measured Eckhaus stability boundaries for Taylor-Couette flow which has been found with two different radius ratios [3,7–9]. Recently, Paap and Riecke [10] calculated the stability boundary for Taylor-Couette flow for an additional radius ratio, $\eta=0.5$, and predicted the existence of a new, short-wavelength instability which supersedes the Eckhaus instability when the system is in a large-wave-number state. Labeling the periodic states by their wave number q, the Eckhaus instability leads to the minimum possible adjustment of q, the loss or addition of one periodic unit [5], whereas the short-wavelength instability results in a relatively large adjustment of q, the loss of multiple periodic units [10]. In this paper, we present an experimental measurement of the stability boundary for a Taylor-Couette system with $\eta=0.5$. We observe dynamics consistent with the existence of a short-wavelength instability, and the measured stability boundary agrees with the calculated one.

The rest of the paper is organized as follows. Section II contains a description of the apparatus and experimental parameters. Section III is a brief discussion of the theory. Sections IV and V present the results of the measurement of the location of the stability boundary and the dynamics of the instability, respectively. Section VI is a summary and conclusion.

II. DEFINITION OF PARAMETERS AND EXPERIMENTAL APPARATUS

We used a standard Taylor-Couette apparatus [3] consisting of two concentric, straight cylinders with a fluid confined between them. The outer cylinder was made of plexiglass, and the inner one of an aluminum core clad with delrin. The inner cylinder was rotated with an angular frequency Ω, and the outer cylinder was held fixed. Below a critical value Ω_c of Ω, the flow is purely azimuthal and shows no axial structure. At Ω_c, the flow undergoes a transition to Taylor vortex flow (TVF), which consists of counter rotating vortices stacked along the axis of the cylinders. The flow pattern is treated as one dimensional, with a wave number

$$q=2\pi/\lambda ,$$

where λ is the axial width of a pair of vortices. The ratio of the inner to outer cylinder radius (radius ratio) was $\eta=0.499$, and the radial gap between the cylinders was $d=1.253$ cm. The cylinder radii were uniform to ± 0.003 cm. The centers of cross sections perpendicular to the axis deviated from a straight line by no more than ± 0.003 cm. The gap contained two nonrotating boundaries made of delrin; one located near each end of the apparatus. The boundaries' axial positions were adjustable by means of two 2.5-mm-diameter stainless-steel rods which passed through seals in the end caps of the apparatus and attached to each boundary. This allowed for changes of the aspect ratio $\Gamma=l/d$, where l is the physical distance between the boundaries, from 28 to 18. During an experimental run, the faces of both boundaries were located at least 5 cm from the ends to thermally isolate the working fluid from the end caps. One boundary was positioned by hand, and the other boundary was positioned with a resolution of 0.005 mm by a stepper motor using a commercial, computer-controlled driver. They were 4.5 cm long and were a sliding fit in the outer cylinder to ensure that the face of the boundary was perpendicular to the axis of the cylinders. As shown schematically in Fig. 1, the gap between the inner cylinder and the inner surface of the boundaries was 0.14 cm over a 0.025-cm-long axial range adjacent to the face of each boundary, and widened to 0.75 cm for the rest of the length of the boundary. This large gap ensured that viscous heating of the fluid was negligible.

The fluid consisted of 50% by volume glycerol in wa-

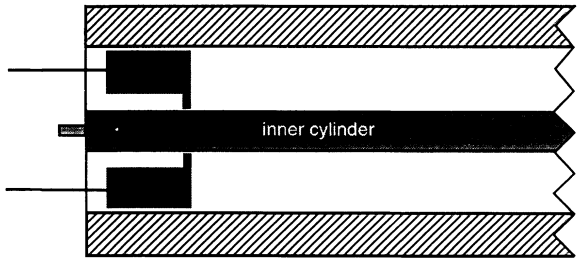

FIG. 1. Schematic diagram, not to scale, of the apparatus showing the shape of the movable boundaries. See the text for the dimensions. The axial position of each boundary is adjustable by means of the two thin stainless-steel rods attached to each boundary as shown.

ter, seeded with either 1% by volume Kalliroscope [11] for flow visualization, or 1 ppm of 1.07μm-diameter polystyrene spheres for use with laser-doppler velocimetry (LDV) [12]. The useful lifetime of the Kalliroscope suspension was increased by adding 0.01% stabilizer [11] to the solution. LDV allows measurement of the axial velocity component of the fluid at a given axial and radial position in the cylinder, but does not allow simultaneous measurement of the velocity at many points along the cylinder axis. To visualize the flow along the entire system at the same instant in time, Kalliroscope was used. This does not allow for a quantitative measurement of the velocity but does reveal the pattern. Ω_c depends on the viscosity of the fluid, which for water varies 2% per degree, and for glycerine varies 9% per degree. To maintain a constant viscosity, the system was temperature controlled by flowing water along the exterior of the outer cylinder, but not through the endcaps. The water was temperature controlled to ± 15 mK, resulting in a stability in Ω_c of 0.1%

It is convenient to define a reduced stress parameter

$$\epsilon=\Omega/\Omega_c-1 \ .$$

As one steps quasistatically through $\epsilon=0$, the pattern that emerges has $q=q_c$ in a system with infinite axial extent. In the finite system with rigid, nonrotating boundaries, there is no sharp bifurcation from Couette flow to TVF [3]. For all values of Ω, the boundaries generate Ekman vortices at each end. This drives vortices in the bulk of the system which have an amplitude that decays exponentially with increasing distance from the ends. Thus, in principle, the entire system is filled with vortices as soon as $\Omega>0$. However, when ϵ is much less than zero, the amplitude of the vortices in the center of the system is too small to detect experimentally. The value of Ω at which vortices are first detected in the center of the system, $\Omega_{\rm on}$, depends on the length l of the system. By measuring $\Omega_{\rm on}$ as a function of l and extrapolating in a well-defined way to infinite l, one infers a value [3] for Ω_c and thus $\epsilon=0$.

For the rest of the paper, we will use nondimensional variables with lengths scaled by the gap d between the cylinders, and time scaled by the viscous diffusion time $t_\nu=d^2/\nu=27$ sec, where ν is the kinematic viscosity. We define the reduced wave number as

$$\tilde{q}=(q-q_c)/q_c \ ,$$

where, for our system [13], $q_c=3.163$.

The wavelength of the pattern was measured in two different ways, depending on the probe of the flow that was being used. During Kalliroscope visualization, a traveling microscope mounted parallel to the axis of the apparatus was used to measure the location of the inflow and outflow boundaries. The wavelength of the pattern is the distance from one outflow (inflow) boundary to the next outflow (inflow) boundary. The average wavelength of the system was measured, discounting one vortex pair at each end so as to exclude the Ekman vortices. The traveling microscope had a 0.05-mm resolution, and the precision in the average wave number was 0.2%. When using LDV, the velocity profile for the central three or four vortex pairs was measured, and the zero crossings were determined. This method had a precision in the average wave number of better than 0.1%.

Originally, our Taylor vortex apparatus consisted of one fixed boundary and one movable boundary. With this setup, states with a uniform wave number were observed for $\tilde{q}>0$ and ϵ near the stability boundary. By employing two movable boundaries, we were able to eliminate the nonuniformity for $\tilde{q}<0.35$, but for values of $\tilde{q}>0.35$ and ϵ near the stability boundary, states with a nonuniform wave number were still observed. The nonuniformity in wave number was spatially distributed so as to cause one half of the system to have an average wave number $q_>$ that was larger than the average wave number q for the entire system. Defining $\Delta\tilde{q}=(q_>-q)/q_c$, states with $\Delta\tilde{q}<0.003$ were considered to have a uniform wave number. For the states with $\tilde{q}>0.35$ and ϵ near the stability boundary, $\Delta\tilde{q}$ reached values as large as 0.035. Because the theory assumes a uniform wave number, such a large nonuniformity makes comparison with predictions difficult. The method used to circumvent this problem is described in Sec. V.

III. THEORETICAL PREDICTIONS

Figure 2 gives theoretical predictions for the stability boundaries in the ϵ-q parameter space for the $\eta=0.5$ Taylor-Couette system [10,13]. Below the neutral curve [13] (solid line), Couette flow is stable. Taylor vortices of infinitesimal amplitude and wave number q grow exponentially for values of ϵ above the solid line. The dashed line gives the stability boundary of fully developed TVF [10]. Within it, states with a finite amplitude are stable. For values of ϵ and q between the solid and dashed lines, Taylor vortex flow is unstable because the growth rate $\sigma(k)$ of infinitesimal perturbations with wave number k is positive for some value of k. One can distinguish between different instabilities according to the

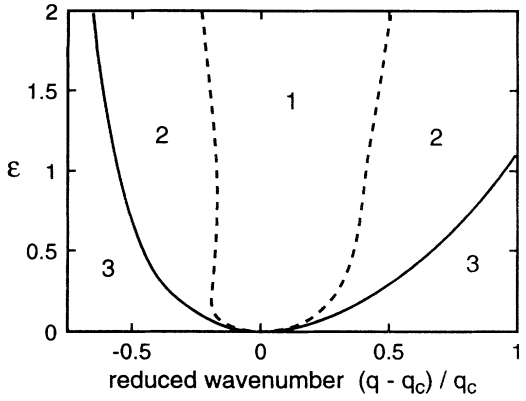

FIG. 2. The stability boundary (dashed line) and the neutral stability boundary (solid line) for radius ratio 0.5. Couette flow is stable with respect to perturbations outside the neutral stability boundary (region 3). Above the neutral stability curve, Taylor vortex flow exists in a range of wave numbers q for each ϵ. States with wave numbers inside the stability boundary (region 1) are stable, and those with wave numbers between the neutral stability boundary and the stability boundary (region 2) have a positive growth rate but are unstable.

value of k for which $\sigma(k)$ first becomes positive. When $\sigma(k)$ first exceeds zero near $k=0$, the instability is of the Eckhaus type [2–6]. The new short-wavelength instability under consideration here yields positive growth rates [10] near $k=q/2$. Two typical $\sigma(k)$ curves for $\eta=0.5$ calculated by Paap and Riecke [10] are plotted in Fig. 3 for states with two different values of q. The value of ϵ for each curve is such that the states are unstable, but close to the stability boundary, i.e., just outside region 1. The dashed line shows that the state with $\tilde{q}=0.369$ is unstable to perturbations with k near zero. This illustrates the standard Eckhaus instabiliity. The state with $\tilde{q}=0.462$ has a growth rate given by the solid line in Fig. 3, and is only unstable to perturbations with k near $q/2$. This is an example of the short-wavelength ($q/2$) instability [10]. The location of the stability boundary in Fig. 2 for a state with wave number q is the value of ϵ at which *either* $k=0$ *or* $q/2$ perturbations first acquire a positive growth rate. The *type* of instability is defined by *which* value of k first acquires a positive growth rate.

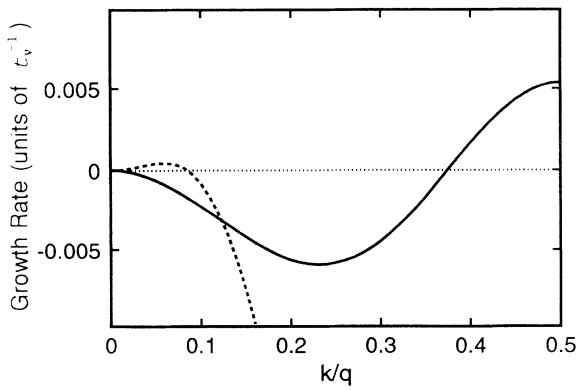

FIG. 3. Perturbation growth rates σ, in units of $(t_v)^{-1}$, vs the wave number of the perturbation (k/q). The curves show the difference between the short-wavelength (solid curve, $\tilde{q}=0.462$, $\epsilon=1.54$) and Eckhaus (dashed curve, $\tilde{q}=0.369, \epsilon=0.555$) instabilities.

The experiments do not directly measure the growth rates of the perturbations. Instead, the nature of the transition from an unstable to a stable state is observed. This depends on $\sigma(k)$, as well as on the nonlinear dynamics of the system. For the Eckhaus case, the experimentally observed transition [3] agrees with the calculations both at the stability boundary and far into the unstable region [5,6]. Near the stability boundary the transition between an unstable and stable state occurs *via* the loss or addition of a single vortex pair [3,5]. Further below the Eckhaus stability boundary, decreasing ϵ for a fixed q, the transition occurs *via* the loss or addition of multiple pairs, with the number of pairs increasing as the distance from the stability boundary increases [6].

Currently, no such detailed calculations exist for the $q/2$ case, but reasonable conjectures about the dynamcis of the transition can be made. The first supposition is that when the $\sigma(k)$ curve is positive only for $k\approx q/2$, every other vortex pair in the system would be lost [10]. Second, one expects the dynamics of the $q/2$ and Eckhaus instabilities to be similar when the system is quenched so far below the stability boundary that the growth rates of the perturbations are positive over a similar range [14]. The growth-rate curves in Fig. 4(a) are examples of an Eckhaus instability (dashed line) and a $q/2$ instability (solid line) for which this occurs [10]. In both cases, perturbations of all wavelengths between $p=k/q=0$ and $p=0.5$ have a positive growth rate, and the perturbations with $p=0.5$ have a growth rate significantly greater than zero. However, as shown in Fig. 4(b), the location in the ϵ-q plane relative to the theoretical stability boundary for the Eckhaus case (triangle) is very different from the $q/2$ case (circle). For the Eckhaus case, there is a significant difference in q between the location of the stability boundary and the value at which perturbations with a wave number $p=0.5$ have a substantial positive growth rate. For the example shown in Fig. 4(b), the difference is 0.7%. For the $q/2$ instability, the difference in q between where only perturbations with $k\approx q/2$ have a positive growth rate and where all perturbations have a positive growth rate is at most [10] 0.2%. Figure 4(c) illustrates the difference in growth-rate curves for three states, all lying very near the circle in Fig. 4(b). In the experiment, the local variation in q was always at least 0.2% for $\tilde{q}>0.35$, making it impossible to probe the region where the only perturbations with positive growth rate were those near $q/2$. Thus it is difficult to establish the nature of the instability unambiguously from experiment. However, sufficiently near the Eckhaus stability boundary we expect to observe the loss or addition of a single vortex pair, and near the $q/2$ stability boundary we expect to observe the loss of multiple vortex pairs. In the latter case, the number of pairs lost should be similar to the number of pairs lost far enough below the Eckhaus stability boundary that $\sigma(k)$ has a maximum near $k=q/2$.

IV. MEASUREMENT OF THE STABILITY BOUNDARY

Figure 5 shows the measured and theoretical [10] stability boundaries for a radius ratio $\eta=0.5$. The line in the region labeled 2 is the predicted $q/2$ instability; the rest of the line is the predicted Eckhaus instability. The value of $\tilde{q}$ for each experimental point is an average of $\tilde{q}$ over the system length, excluding one roll pair from each end.

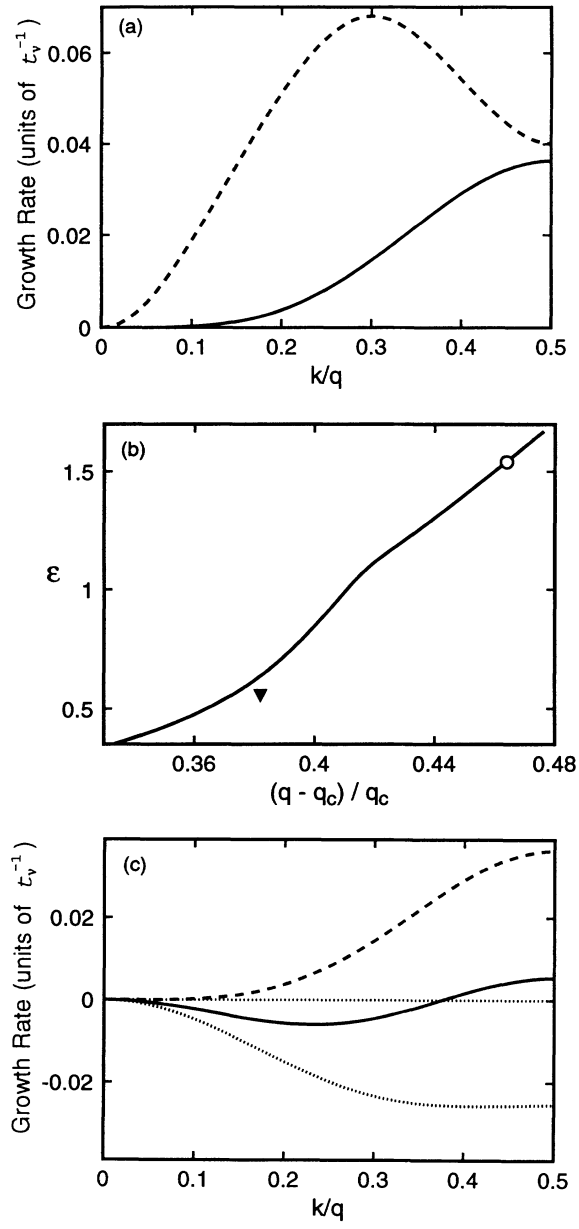

FIG. 4. (a) Growth-rate curves for a state with $\tilde{q}=0.464$ and $\epsilon=1.54$ ($q/2$ instability, solid line) and a state with $\tilde{q}=0.382$ and $\epsilon=0.555$ (Eckhaus instability, dashed line). Both states are unstable. (b) Location of $(\tilde{q},\epsilon)=(0.464,1.54)$ (open circle) and $(\tilde{q},\epsilon)=(0.382,0.555)$ (triangle) with respect to the theoretical stability boundary (solid line). (c) Growth-rate curves for three states near the $q/2$ instability with very slightly different wave numbers at $\epsilon=1.54$. The state with $\tilde{q}=0.461$ (dotted line) is stable. The states with $\tilde{q}=0.462$ (solid line) and $\tilde{q}=0.464$ (dashed line) are both unstable.

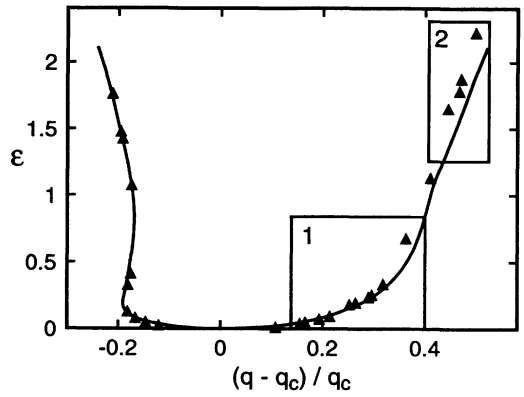

FIG. 5. The observed stability boundary (triangles) and the calculated stability boundary (solid curve) for radius ratio $\eta=0.5$. Region 2 is predicted to span the new $q/2$ instability. The rest of the curve is predicted to be determined by the Eckhaus instability.

The experiment was done in the following manner. The movable boundary not being controlled by a stepper motor was positioned 10 cm from the corresponding end of the cylinder when creating states with $q>q_c$, and 5 cm for states with $q<q_c$. For creating states with $q>q_c$, the stepper-motor-controlled boundary was positioned as close to the corresponding end of the cylinder as possible, giving an aspect ratio $\Gamma=26$. For creating states with $q<q_c$, the stepper-motor-controlled boundary was positioned so that $\Gamma=18$. Once the boundaries were positioned, an integer number of vortex pairs was created by rapidly varying ϵ from well below 0 to a value near 1. In general, this produced betweeen 13 and 15 vortex pairs for $q>q_c$, and between 10 and 12 vortex pairs for $q<q_c$. Once the vortices had equilibrated, ϵ was adjusted to be well above the theoretical stability boundary for the desired q. Then, the stepper-motor-controlled boundary was quasistatically moved in for $q>q_c$ or out for $q<q_c$, which compressed or stretched the vortices, respectively, until the desired q was reached. The final result was to have the vortices confined between the boundaries, which were roughly the same distance from the ends of the apparatus.

Once the system was in a state with the desired value of q, ϵ was adjusted so as to bring the system close to the instability. Near the instability, steps in ϵ of 0.005 were taken every 2 h, or $270t_v$. After each step, if one or more vortex pairs were lost or gained, the average of the current and previous values of ϵ was declared the instability point. If no adjustment occurred, the next step was made. Once an adjustment occurred, the new state was used as an initial state, and the above procedure of adjusting ϵ was repeated.

For most of the predicted Eckhaus boundary, the agreement between experiment and theory is excellent, and the loss or addition of a single vortex pair was observed as expected. For q values where the boundary is predicted to be governed by the $q/2$ instability, we also observed the loss of only a single vortex pair, instead of

the expected multiple-pair loss. Figure 5 shows that there exists a significant discrepancy between experiment and theory as to the location of the stability boundary for points with $\tilde{q} > 0.350$ [see Figs. 7(a) and 7(b) for expanded views of the boxed sections in Fig. 5]. This discrepancy can be understood in terms of the nonuniformity in wave number discussed in Sec. II.

The effects of a nonuniform wave-number distribution are illustrated by the space-time plot in Fig. 6 which shows the transition from 14 to 13 vortex pairs at $\tilde{q}=0.470$ and $\epsilon=1.88$. The wavelength of the pattern, as defined in Sec. II, is the axial width of a vortex pair and is labeled by λ in Fig. 6. Because the Kalliroscope signal does not differ much for inflow and outflow boundaries, a vortex pair corresponds to a pair of peaks in the image. The vertical dashed lines in Fig. 6 divide the system into two parts of equal length. For this case, $\Delta\tilde{q}=0.035$, which corresponds to a $\tilde{q}$ for the left half of the system of 0.505. Figure 6 also shows that the vortex pair loss at $300t_\nu$ occurs in the left half of the system. If only this half of the system is considered, one can see from Fig. 7(b) that $\tilde{q}=0.505$ and $\epsilon=1.88$ (shown as an open circle) are in the unstable region. The pair loss occurred when this region of the system had an unstable wave number. This was true for all of the measured stability boundary points which disagreed with theory. However, the size of the region which was locally unstable depended on $\tilde{q}$ and ϵ.

The nonuniform wave number for states with $\tilde{q} > 0.350$ can also account for the observation of a single-pair loss in region 2 of Fig. 5, instead of the predicted multiple-pair loss. Because the transition always occurs when some neighborhood around the pair with the largest wave number crosses the theoretical stability boundary, we assume that the wave-number adjustment results from the system being "locally" unstable [15]. The dynamics of this local transition cannot be used to distinguish between the Eckhaus and $q/2$ instabilities because, in the immediate neighborhood of a vortex pair, the loss of every other pair is the loss of one vortex pair. To compare the Eckhaus and $q/2$ instabilities, the dynamics of a uniform state at the stability boundary need to be studied. To accomplish this, we took advantage of the fact that the nonuniformity takes longer to develop than does either the Eckhaus or $q/2$ instabilities. We report our results in Sec. V. It is possible that the nonuniformity is an intrinsic instability, and not simply due to an inhomogeneity in the system. However, for the rest of the paper, "instability" will refer specifically to a wave-number adjustment process through the loss or addition of a vortex pair or pairs.

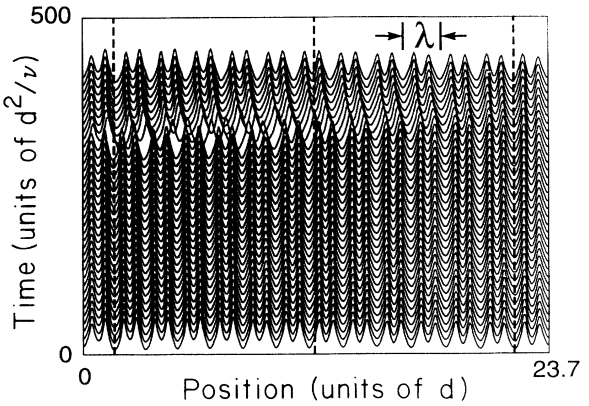

FIG. 6. Time series of scanlines of TVF for $\tilde{q}=0.470$, $\epsilon=1.88$, and $\Delta\tilde{q}=0.035$. The variation of each scanline is proportional to the intensity of the Kalliroscope signal. The three vertical dashed lines are a guide to the eye, and separate the system into two halves. The left half has a higher $\tilde{q}$, and this is the half in which the transition occurs.

V. DYNAMICS OF UNIFORM STATES

Using quasistatic measurements, the local nature of the transition for $\tilde{q} > 0.350$ complicated attempts to distinguish the Eckhaus and $q/2$ instabilities, but the *location* of the experimental and theoretical boundaries agreed when the nonuniform wave number was taken into account. To observe the dynamics of the instability for a uniform state, we performed quenches as follows. A state with the desired average wave number was created, as for the quasistatic measurements, and ϵ was set far enough above the stability boundary so that the steady state had a uniform wave number. Then the value of ϵ was stepped to a value at or below the quasistatically measured stability boundary. Instead of changing ϵ in a single step, some quenches were performed by ramping ϵ at dimensionless rates $t_\nu d\epsilon/dt$ ranging from 0.03 to 0.14. Independent of the quench method, the wave number of the state remained uniform to better than 0.4% as ϵ was changed. Once the final value of ϵ was reached, the evolution of the system was recorded as a time series of Kalliroscope images. The evolution of the system was also independent of the quench method.

Quenches were performed in the two boxed regions of the ϵ-$\tilde{q}$ plane labeled in Fig. 5. Region 1 is predicted to be Eckhaus unstable, and region 2 is predicted to be $q/2$ unstable [10]. Figures 7(a) and 7(b) show the number of pairs lost in each quench for these regions, respectively. For $\tilde{q} > 0.350$, the quasistatistically measured boundary is significantly above the theoretical boundary described previously in Sec. IV. For these values of q, we performed quenches to values of ϵ between the measured and theoretical boundaries. The behavior of these quenches was consistent with the quasistatic measurements. The wave number of the system devleoped a nonuniform distribution, and a single pair was lost when the state became locally unstable. In contrast, for quenches at or below the *theoretical* stability boundary, the loss of a vortex pair or pairs occurred on a faster time scale than the evolution of a nonuniform wave-number distribution. The number of pairs lost for these quenches was independent of the location of the quasistatically measured boundary relative to the theoretical boundary. However, the number of pairs lost was dependent on whether the quench was in region 1 or 2 of Fig. 5.

For quenches in region 1, we observed behavior consistent with the Eckhaus instability as shown in Fig. 7(a). We observe the loss of a single vortex pair when quench-

ing to the theoretical boundary (solid line). For quenches further into the unstable reigon, there is an increase in the number of pairs lost from one to two to three as the quench depth is increased. For the quenches in region 2, we observed behavior consistent with that expected for the $q/2$ instability as shown in Fig. 7(b). Quenches to the theoretical boundary result in the loss of three pairs, as was seen in region 1 *only far below* the Eckhaus boundary. Figure 8 shows gray-scaled space-time plots for four quenches near the boundary. The first three quenches shown are from region 2 of Fig. 5, and the fourth quench is from region 1. Even for the quenches to the theoretical boundary, a small nonuniformity in the wave number began to develop. If this had dominated the transition, the initial pair loss would have occurred in the region of the largest local wave number, as it did for the quasistatic measurements with $\bar{q} > 0.350$ (see Fig. 6). For the first three plots in Fig. 8, the left half of the system has a slightly larger average wave number, but the first pair loss does not always occur in that half of the system. Furthermore, the transition occurs throughout the system, not locally. This demonstrates that the instability is not dominated by nonuniformities in $\bar{q}$. The fourth plot in Fig. 8 shows a typical Eckhaus transition and illustrates the differences between the quenches in regions 1 and 2. In addition to the number of pairs lost, the dynamics of the pair loss varies. For higher values of $\bar{q}$, the pair loss is more precipitous, as shown in more detail in Fig. 9.

We also performed quenches starting with an initial state that had a nonuniformity in wave number greater

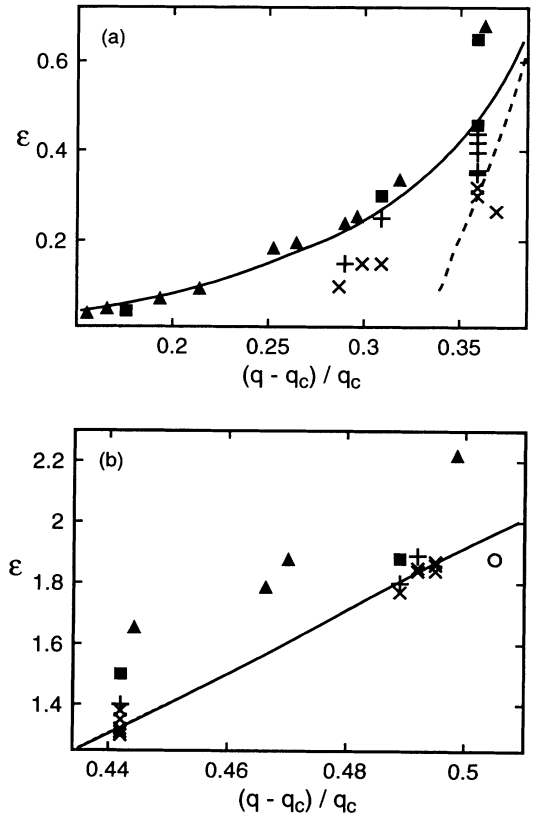

FIG. 7. (a) Results of quenches for which the instability was predicted to occur via the Eckhaus mechanism (region 1 of Fig. 5). Single-pair losses (squares) occur for quenches close to the theoretical boundary (solid curve), and for quenches anywhere between the quasistatically measured boundary (triangles, see Fig. 5) and the theoretical boundary. Two- (plus signs) and three- (crosses) pair losses occur for quenches below the theoretical boundary. For $\bar{q}=0.36$, the three-pair losses occur for quenches made at or below the location where perturbations with wave number $q/2$ acquire a positive growth rate (dashed curve). (b) Results of quenches for which the instability was predicted to occur via the short-wavelength ($q/2$) instability (region 2 of Fig. 5). Here single-pair losses (squares) occur for quenches between the quasistatically measured (triangles, see Fig. 5) and theoretical (solid curve) stability boundaries, but only after a state of spatially nonuniform wave number developed. For quenches made to points at and below the theoretical boundary, we observed two- (plus sign) and three- (crosses) pair losses when the wave number was uniform.

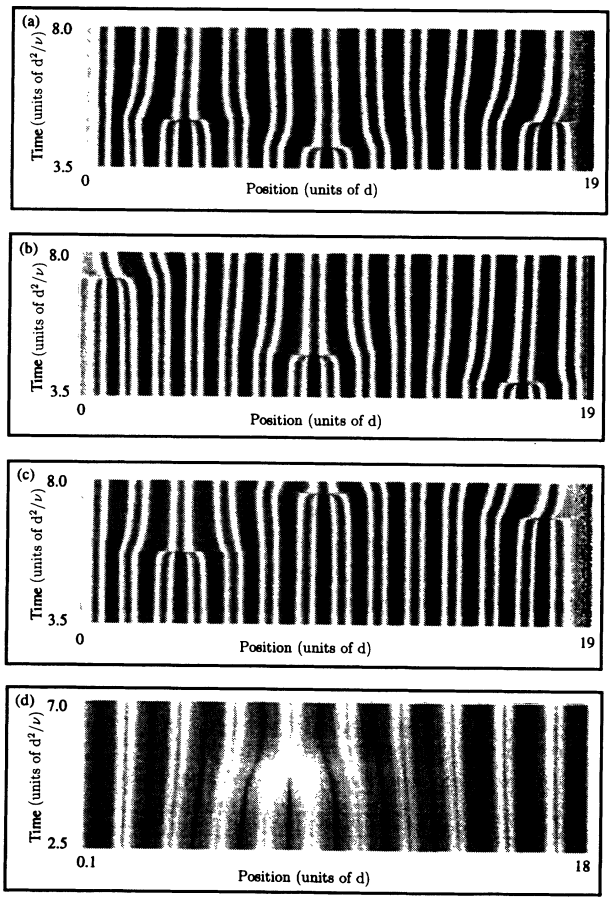

FIG. 8. Gray-scaled space-time plots of the evolution of the system after a quench from a uniform state. For images (a)–(c), the instability is predicted to be $q/2$, while it should be of the Eckhaus type for image (d). For all four quenches, $t=0$ is the time that the final value of ϵ was reached. (a) and (b) are for quenches from $\epsilon=2.38$ to 1.84 and 1.85, respectively, for a state with average reduced wave number $\bar{q}=0.495$. (c) is for a quench from $\epsilon=2.34$ to 1.84 with $\bar{q}=0.492$, and (d) is for a quench from $\epsilon=0.14$ to 0.05 with $\bar{q}=0.174$. The theoretical boundary is at $\epsilon=1.866$ for $\bar{q}=0.495$, $\epsilon=1.840$ for $\bar{q}=0.492$, and $\epsilon=0.062$ for $\bar{q}=0.174$.

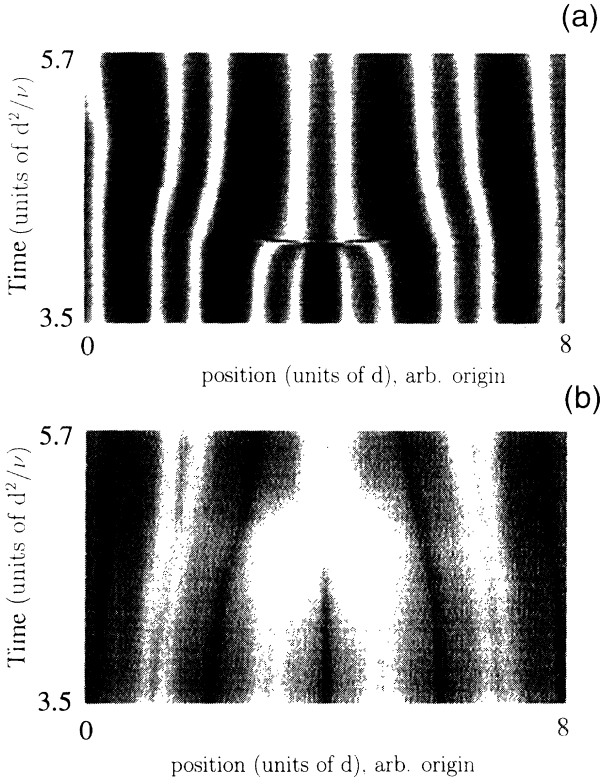

FIG. 9. Magnified view of two pair losses. (a) is a magnified view of the central pair loss of Fig. 8(a), $(\tilde{q},\epsilon)=(0.495,1.84)$, and 9(b) is a magnified view of the pair loss in Fig. 8(d), $(\tilde{q},\epsilon)=(0.174,0.05)$.

than 0.5%. Because the nonuniformity was present before the quench, it should have dominated the dynamics. Using this initial state, quenches to values of ϵ at or below the predicted $q/2$ boundary exhibited the loss of only a single vortex pair, which occurred in the region of largest wave number, demonstrating that there is a difference between uniform and nonuniform systems. Therefore, by creating a *uniform* initial state at the theoretical boundary, we sufficiently suppressed the effects of the nonuniform wave number, enabling the observation of the dynamics of the instability. We observed the two types of transitions discussed in Sec. III: the loss of a single vortex pair near the Eckhaus stability boundary, and the loss of multiple (three) vortex pairs far below the Eckhaus boundary and near the $q/2$ stability boundary.

Recently, Riecke [14] predicted that the $q/2$ instability should be operative for the Taylor-Couette system with a radius ratio $\eta=0.75$. For this system, we have observed behavior consistent with the behavior observed near the predicted $q/2$ stability boundary in the $\eta=0.5$ system. For the $\eta=0.75$ system, the number of vortex pairs was between 28 and 30, and quenches at or below the predicted $q/2$ instability resulted in the loss of six or seven vortex pairs. This is the same relative change of q observed in the $\eta=0.5$ system. Figure 10 is an example of a space-time plot for such a quench, but a detailed study of the stability boundary remains to be done for $\eta=0.75$

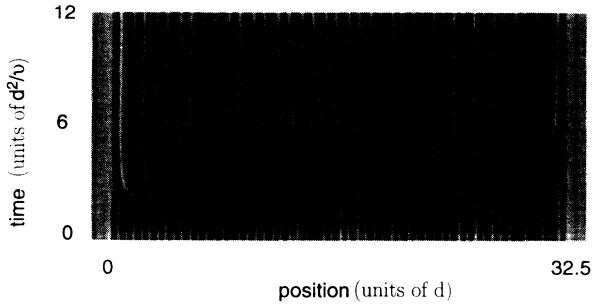

FIG. 10. Gray scaled space-time plot showing the evolution of the system following a quench using the radius ratio $\eta=0.75$ apparatus. The quench was from $\epsilon=2.81$ to 1.96 for a state with average reduced wave number $\tilde{q}=0.66$. The theoretical boundary is at $\epsilon=2.00$ for this value of $\tilde{q}$, and is predicted to be determined by the $q/2$ instability.

VI. SUMMARY

In Sec. IV, we reported our measurement of the stability boundary for the Taylor-Couette system with a radius ratio 0.5. To our knowledge, a measurement of the stability boundary for this radius ratio has not previously been reported. We found good agreement with the theoretical boundary calculated by Paap and Riecke [10] in the range from near $\epsilon=0$ up to $\epsilon\approx 2$. Especially for negative $\tilde{q}$ the agreement was excellent, and the data even reproduced the predicted reentrant nature of the stability boundary. For positive $\tilde{q}$, equally good agreement was obtained up to $\tilde{q}=0.25$. For even larger $\tilde{q}$, the apparent differences between theory and experiment can be accounted for by a nonuniformity in the wave number of the states which develops in this parameter range. In Sec. V, we discussed the quenches performed to study the dynamics of the instabilities which enabled us to distinguish between the global dynamics of the wave-number transitions in the uniform system and local transitions induced by a nonuniform wave number. Two types of system wide dynamics were observed for uniform states at the theoretical boundary which distinguished the Eckhaus instability with its single-vortex-pair loss from the new instability which leads to multiple-vortex-pair loss. To our knowledge, this is the first experimental observation of this new instability, and the behavior of the new instability is consistent with the predicted $q/2$ instability [10,14]. We also saw very convincing evidence for this instability in an $\eta=0.75$ system.

In the experiments performed by Dominguez-Lerma, Cannell, and Ahlers [3], a discrepancy between theoretical and measured stability boundaries was observed for $\tilde{q}>0$, but for $\tilde{q}<0$ excellent agreement was found between theory and experiment. In these experiments, a single movable boundary was used, and a nonuniform wave number was observed for $\tilde{q}>0$. One asymmetry between the $\tilde{q}>0$ states and $\tilde{q}<0$ states which could account for these results is in the method used to generate the states: states with $\tilde{q}>0$ have the movable boundary away from its corresponding endcap, while states with $\tilde{q}<0$ have the movable boundary close to its corresponding endcap. Our use of two movable boundaries eliminat-

ed this asymmetry, because the second movable boundary could be placed the same distance from the endcap as the one used to create the correct wave number. This eliminated the nonuniform wave number for $\tilde{q} < 0.350$, and we found agreement with theory in this range of $\tilde{q}$. These observations are consistent with thermal heating at the ends being the source of nonuniformities in both experiments. With two movable boundaries or one movable boundary and $\tilde{q} < 0$, the working fluid is heated more or less symmetrically from both ends. No significant nonuniformity in wave number develops, and there is agreement between theory and experiment. With one movable boundary and $\tilde{q} > 0$, the working fluid is heated asymmetrically from the ends which results in a nonuniform wave number and disagreement with the theory which applies to the uniform state.

Because the nonuniformity in wave number persisted in the present experiment for $\tilde{q} > 0.350$, we believe it is possible that this nonuniformity is an intrinsic instability. The Taylor-Couette system can be described by a phase-diffusion equation in which the diffusion constant goes to zero at the stability boundary [5]. For certain values of the coefficients in the phase-diffusion equation, there exist states with a localized nonuniformity in the wave number [16–19]. In the Taylor-Couette system [14], these states might exist for $\tilde{q} > 0.350$ and not exist for $\tilde{q} < 0.350$. On the other hand, for $\tilde{q} > 0.350$ the system may simply be more susceptible to the small experimental asymmetries remaining. Both of these explanations for the nonuniformity in wave number are plausible. For large $\tilde{q}$ the phase diffusivity remains small further away from the stability boundary than does [20] for smaller $\tilde{q}$, and a system with a small diffusivity is more sensitive to external imperfections. The use of two boundaries could have reduced the asymmetry in the heating enough to remove the problem for $\tilde{q} < 0.350$, but for $\tilde{q} > 0.350$ the system could be sensitive enough that it still responded to some remaining small asymmetric heating. More work is needed to determine whether or not the observed nonuniform wave number is caused by an intrinsic instability or is the result of the smaller diffusion constant and experimental imperfections.

ACKNOWLEDGMENTS

We thank Hermann Riecke for many useful discussions and for providing the data for Figs. 3 and 4. We also thank Li Ning, Ken Babcock, and Marco Dominguez-Lerma for helpful discussions about the experimental details. This work was supported by the National Science Foundation through Grant No. DMR91-17428. M.D. acknowledges support from the Office of Naval Research.

[1] A sizable literature now exists dealing with this system. A comprehensive review has been given by R. C. DiPrima and H. L. Swinney, in *Hydrodynamic Instabilities and Transitions to Turbulence,* edited by H. L. Swinney and J. P. Gollub (Springer, Berlin, 1981). Important early papers in this field are numerous, but particularly noteworthy are D. Coles, J. Fluid Mech. **21**, 385 (1965); H. A. Snyder, *ibid.* **35**, 273 (1969); J. E. Burkhalter and E. L. Koschmieder, Phys. Fluids **17**, 1929 (1974).

[2] W. Eckhaus, *Studies in Nonlinear Stability Theory* (Springer, New York, 1965).

[3] M. A. Dominguez-Lerma, D. S. Cannell, and G. Ahlers, Phys. Rev. A **34**, 4956 (1986).

[4] H. Riecke and H. G. Paap, Phys. Rev. A **33**, 547 (1986).

[5] L. Kramer and W. Zimmermann, Physica (Amsterdam) D **16**, 221 (1985).

[6] L. Kramer, H. R. Schober, and W. Zimmermann, Physica (Amsterdam) D **31**, 212 (1988).

[7] D. S. Cannell, M. A. Dominguez-Lerma, and G. Ahlers, Phys. Rev. Lett. **50**, 1365 (1983).

[8] R. Heinrichs, G. Ahlers, and D. S. Cannell, Phys. Rev. Lett. **56**, 1794 (1986).

[9] G. Ahlers, D. S. Cannell, M. A. Dominguez-Lerma, and R. Heinrichs, Physica **23D**, 202 (1986).

[10] H. G. Paap and H. Riecke, Phys. Rev. A **41**, 1943 (1990).

[11] Kalliroscope Corporation, P. O. Box 60, Groton, MA 01450, rheoscopic liquid AQ-1000 and stabilizer. See also P. Matisse and M. Gorman, Phys. Fluids **27**, 759 (1984).

[12] R. Heinrichs, D. S. Cannell, G. Ahlers, and M. Jefferson, Phys. Fluids **31**, 250 (1988).

[13] M. A. Dominguez-Lerma, G. Ahlers, and D. S. Cannell, Phys. Fluids **27**, 856 (1984).

[14] H. Riecke (private communication).

[15] Instabilities in spatially nonuniform systems have been investigated previously for wavy Taylor vortex flow (Ref. [21]) and Rayleigh-Bénard convection (Ref. [22]). In those cases, transitions occurred close to the point where the wave number *locally* crossed the stability boundary of the uniform system.

[16] R. J. Deissler, Y. C. Lee, and H. R. Brand, Phys. Rev. A **42**, 2101 (1990).

[17] H. R. Brand and R. J. Deissler, Phys. Rev. Lett. **63**, 508 (1989).

[18] H. R. Brand and J. E. Wesfreid, Phys. Rev. A **39**, 6319 (1989).

[19] H. Riecke, Europhys. Lett. **11**, 213 (1990).

[20] H. Riecke, Ph.D. thesis, Universität Bayreuth, Bayreuth, W. Germany, 1986 (unpublished).

[21] G. Ahlers, D. S. Cannell, and M. A. Dominguez-Lerma, Phys. Rev. A **27**, 1225 (1983).

[22] M. S. Heutmaker and J. P. Gollub, Phys. Rev. A **35**, 242 (1987).

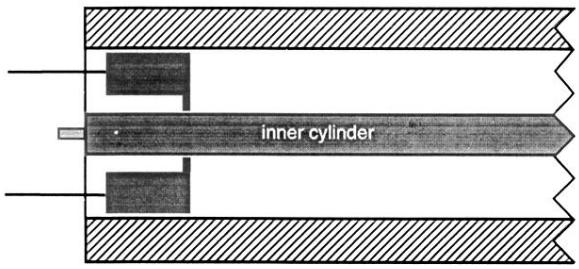

FIG. 1. Schematic diagram, not to scale, of the apparatus showing the shape of the movable boundaries. See the text for the dimensions. The axial position of each boundary is adjustable by means of the two thin stainless-steel rods attached to each boundary as shown.

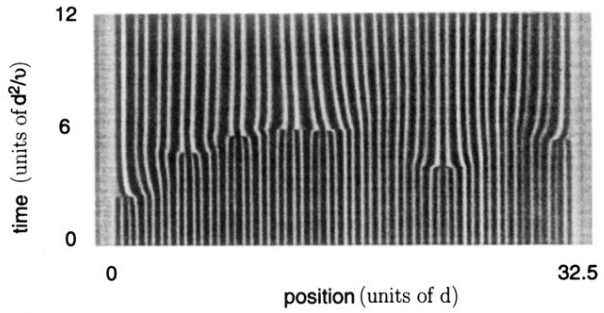

FIG. 10. Gray scaled space-time plot showing the evolution of the system following a quench using the radius ratio $\eta=0.75$ apparatus. The quench was from $\epsilon=2.81$ to 1.96 for a state with average reduced wave number $\tilde{q}=0.66$. The theoretical boundary is at $\epsilon=2.00$ for this value of $\tilde{q}$, and is predicted to be determined by the $q/2$ instability.

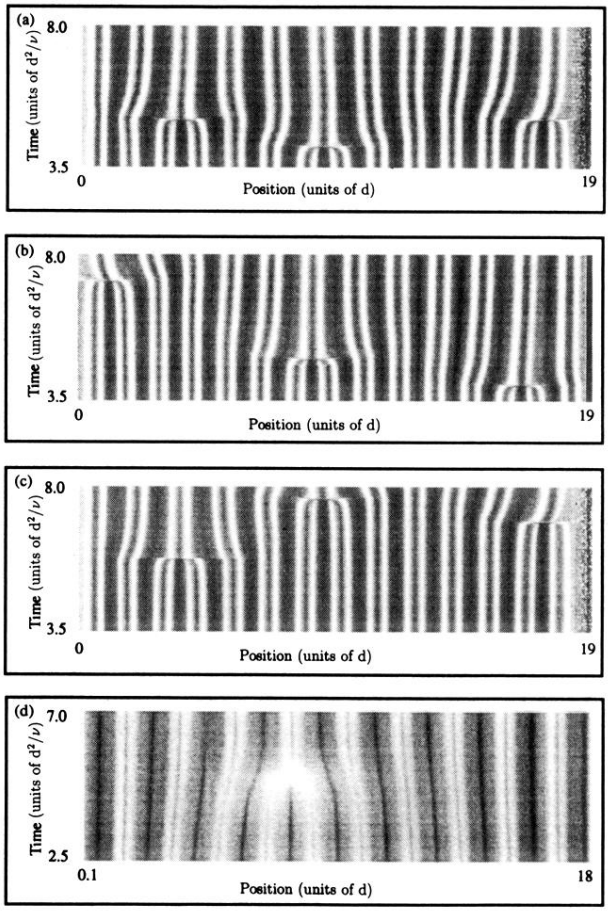

FIG. 8. Gray-scaled space-time plots of the evolution of the system after a quench from a uniform state. For images (a)–(c), the instability is predicted to be $q/2$, while it should be of the Eckhaus type for image (d). For all four quenches, $t=0$ is the time that the final value of ϵ was reached. (a) and (b) are for quenches from $\epsilon=2.38$ to 1.84 and 1.85, respectively, for a state with average reduced wave number $\bar{q}=0.495$. (c) is for a quench from $\epsilon=2.34$ to 1.84 with $\bar{q}=0.492$, and (d) is for a quench from $\epsilon=0.14$ to 0.05 with $\bar{q}=0.174$. The theoretical boundary is at $\epsilon=1.866$ for $\bar{q}=0.495$, $\epsilon=1.840$ for $\bar{q}=0.492$, and $\epsilon=0.062$ for $\bar{q}=0.174$.

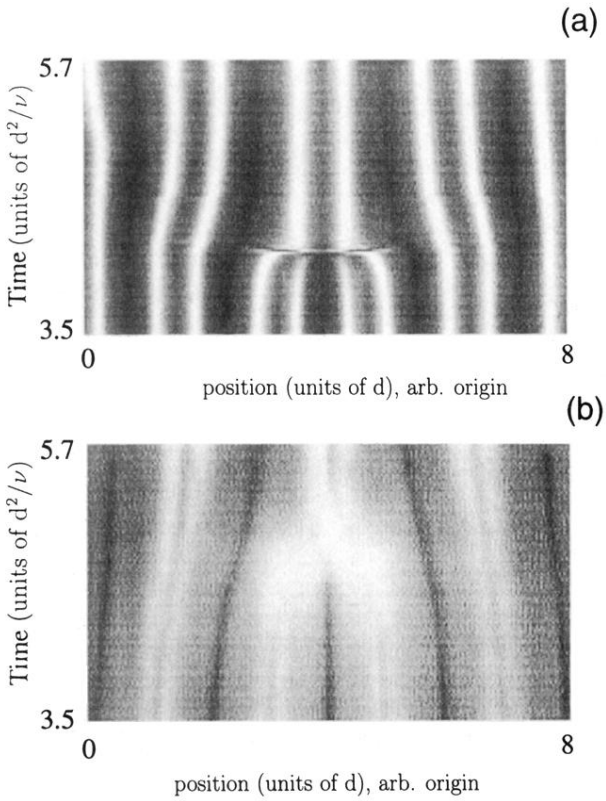

FIG. 9. Magnified view of two pair losses. (a) is a magnified view of the central pair loss of Fig. 8(a), $(\tilde{q},\epsilon)=(0.495,1.84)$, and 9(b) is a magnified view of the pair loss in Fig. 8(d), $(\tilde{q},\epsilon)=(0.174,0.05)$.